JACS
JOURNAL OF THE AMERICAN CHEMICAL SOCIETY

COMMUNICATION

pubs.acs.org/JACS

Determination of Quasi-Fermi Levels across Illuminated Organic Donor/Acceptor Heterojunctions by Kelvin Probe Force Microscopy

David J. Ellison, Jung Yong Kim, Derek M. Stevens, and C. Daniel Frisbie*

Department of Chemical Engineering and Materials Science, University of Minnesota, 421 Washington Avenue SE, Minneapolis, Minnesota 55455, United States

Supporting Information

ABSTRACT: Using Kelvin probe force microscopy (KFM), we have measured the electrochemical potentials across indium tin oxide/organic and donor/acceptor heterojunctions in the dark and under illumination with white light. We have found that the photovoltage generated across these heterojunctions is strongly correlated with the difference between the respective HOMO and LUMO levels of the donor and acceptor and also very closely approximates measured open-circuit voltages in completed solar cells. These results imply that KFM tracks the Fermi level positions within the donor and acceptor layers under photoexcitation. Overall, these results demonstrate the utility of KFM for understanding potential profiles across active layers in planar-heterojunction organic solar cells.

Understanding the spectrum of factors impacting the open-circuit voltage (V_{OC}) in organic photovoltaic (OPV) cells remains an important goal in renewable energy research.[1−3] It is generally established that the positions of the HOMO of the donor (D) and the LUMO of the acceptor (A) play a key role in determining V_{OC}: $V_{OC} = E^{A}_{LUMO} - E^{D}_{HOMO} - \Delta$, where Δ is an empirically determined parameter often attributed to energetic loss mechanisms.[4−7] More precisely, V_{OC} should reflect the difference in quasi-Fermi levels (chemical potentials) for electrons in the donor and acceptor layers under illumination.[1,8,9] It is therefore highly desirable to understand how the positions of the quasi-Fermi levels at D/A heterojunctions depend on the white-light illumination intensity and the choice of donor and acceptor materials. The energetic offset between the donor and acceptor quasi-Fermi levels under illumination represents the maximum electrochemical potential that can be generated. In operating OPV cells, however, the quasi-Fermi level positions at the critical charge-separating interfaces are not accessible because of the cell architecture, which involves multiple layers and contacts.

In this work, we employed Kelvin probe force microscopy (KFM)[10−13] to record potentials across D/A heterojunctions in the dark and under illumination, as shown in Figure 1. The heterojunctions were based on layers of well-known donors and C_{60} as the acceptor (Figure 1c),and the transparent conductor indium tin oxide (ITO) served as the contact to the donor layer; the final structure can be described as ITO/donor/C_{60}. The goal was to measure the potential difference between the exposed acceptor or donor layer and the underlying metal contact. The structures can be viewed as photocapacitors, that is, the potential difference across the stack is a function of light intensity and donor type. We found that the photovoltage measured by KFM depends linearly on the donor HOMO level position and also that there is a direct correlation between the photovoltage and the measured V_{OC} for operational cells based on these materials. The results indicate that KFM can measure the quasi-Fermi level positions of the donor and acceptor layers under illumination. In turn, knowledge of these positions reflects the magnitude of V_{OC} for a given D/A pair. Quasi-Fermi levels are also useful for modeling of OPV devices. For example, if the electronic density of states is known, the quasi-Fermi level positions allow the carrier densities in the layers to be calculated. Overall, our findings indicate that KFM will be a useful tool for understanding the generation of electrochemical potentials across OPV heterojunctions.

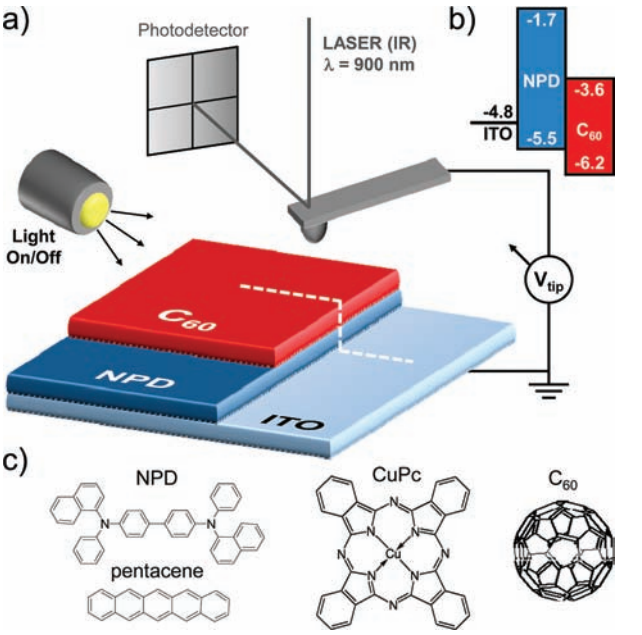

Figure 1. (a) Schematic representation of the KFM setup to map the potential of layered organic heterostructures in the dark and under illumination. Donor/C_{60} (acceptor) layers were thermally evaporated onto ITO in a staggered geometry to visualize the change in potential for each layer individually. (b) Energy level diagram for ITO/NPD/C_{60}. (c) Chemical structures of common NPD, pentacene, and CuPc donors and C_{60} acceptor.

Received: April 14, 2011
Published: August 01, 2011

dx.doi.org/10.1021/ja2034574 | J. Am. Chem. Soc. 2011, 133, 13802–13805

Figure 1 depicts the experimental setup for the KFM measurements, wherein a conductive probe scans across D/A layers that have been vapor-deposited sequentially onto ITO. For irradiation, an optical fiber was placed ~3 mm away from the sample. The fiber was connected to a halogen bulb with variable knob positions calibrated to a measured white-light intensity curve [see the Supporting Information (SI)].[14] The model donor materials NPD, CuPc, and pentacene and the model acceptor C_{60} were chosen in part for their particularly low absorbance in the IR in order to minimize optical pumping from the 900 nm IR laser used to detect cantilever deflection in the atomic force microscopy (AFM) apparatus (Figure 1a). The respective energy levels for the NPD/C_{60} junction are shown in Figure 1b.[15,16]

ITO/donor/C_{60} samples were prepared by sequential thermal deposition of the donor and C_{60} onto ozone-treated ITO[17] inside an inert-atmosphere glovebox with oxygen levels of <2 ppm. The samples were then immediately transferred via an airtight, argon-filled container to a second glovebox that housed the KFM instrument. All of the KFM measurements were performed in under 4 h using a Veeco Instruments Nanoscope IIIA multimode atomic force microscope with probes from Mikromasch USA (NSC18, Pt-coated, resonant frequency 60−90 kHz, k = 2−5.5 N/m, R_C = 25 nm). We performed KFM in a two-pass noncontact lift mode.[12] In the first pass, topography was recorded; in the second pass, the probe was held at a constant height of 100 nm above the sample surface, and the sample potential was recorded. The KFM probe and ITO substrate were electrically connected and thereby capacitively coupled. The electrostatic force between the tip and the sample due to inherent Fermi level differences was nulled by biasing the probe (V_{tip}) until its potential matched the sample potential (ϕ).

Figure 2a shows a schematic illustration of the ITO/NPD/C_{60} heterostructure under illumination. In the absence of a cathode (dashed box), the circuit is incomplete, and electrons cannot leave the stack (i.e., no steady-state direct current flows). For this incomplete circuit, exciton formation and splitting would be expected to result in a steady-state buildup of space charge across the device. Measuring ϕ in the dark and light allowed us to observe and quantify this effect, as shown in Figure 2b for an NPD (40 nm)/C_{60} (40 nm) junction on ITO. In the dark, ϕ for C_{60} with respect to ITO was approximately −300 mV (black curve). Similar measurements across the bare donor layer, ITO/NPD, showed that ϕ for NPD with respect to ITO was approximately −100 mV (data not shown). These potentials reflect the dark-state contact potential differences (CPDs) across the ITO/NPD and NPD/C_{60} interfaces and are consistent with previous measurements of CPDs by photoelectron spectroscopy.[18,19]

Under ~300 mW/cm^2 illumination, ϕ for the top C_{60} layer became significantly more negative (Figure 2b). A negative shift across the NPD/C_{60} interface is expected due to exciton splitting and donor-to-acceptor electron transfer (Figure 2a). This charge transfer process produces negative space charge in the acceptor layer and explains the negative sign of the C_{60} potential. The total photovoltage across the illuminated bilayer was $\Delta\phi_{ITO/NPD/C_{60}} = \phi_{C_{60}} - \phi_{ITO} = -0.83$ V, the absolute value of which is strikingly close to the V_{OC} of 0.9 V measured for an operational solar cell based on these materials (see the SI). This observation will be discussed in more detail later.

$\Delta\phi_{ITO/NPD/C_{60}}$ as a function of light intensity is shown in Figure 2c. It is clear that $\Delta\phi_{ITO/NPD/C_{60}}$ nearly saturates, similar to the trend expected for V_{OC}, which classically displays a

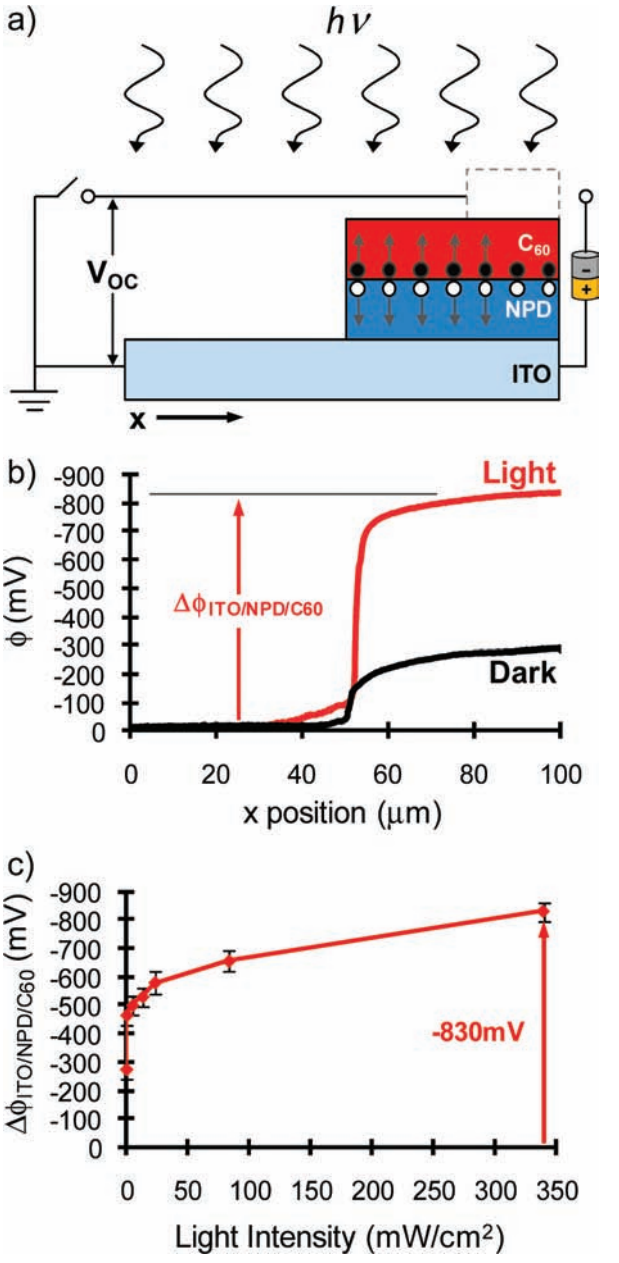

Figure 2. (a) Profile of the bilayer OPV cell showing electrons and holes after exciton splitting, where the carrier distribution reaches a steady-state open-circuit value. (b) Potential line scan of a NPD (40 nm)/C_{60} (40 nm) bilayer device in the dark (black curve) and under ~300 mW/cm^2 illumination (red curve). (c) Photovoltage $\Delta\phi_{ITO/NPD/C_{60}}$ for the NPD/C_{60} bilayer as a function of light intensity. $\Delta\phi_{ITO/NPD/C_{60}}$ is the potential of the C_{60} layer relative to ITO. We note that potential for the bilayer in (a) does not plateau for tens of μm from the organic layer step-edge. This effect is primarily due to sample masking and AFM cantilever-to-sample alignment issues at the interface (see the SI).

logarithmic dependence on light intensity (see the SI).[20,21] Thus, it is clear that KFM is sensitive to charge dissociation and charge buildup across D/A interfaces, consistent with previous electric force microscopy studies of spin-coated polymer D/A layers.[22]

To aid in the interpretation of $\Delta\phi_{ITO/NPD/C_{60}}$, we further studied different D/A combinations in which the donor materials (pentacene, CuPc, NPD) were changed systematically while keeping C_{60} as the acceptor. Important material properties are

dx.doi.org/10.1021/ja2034574 |J. Am. Chem. Soc. 2011, 133, 13802–13805

Table 1. Properties of Donor and Acceptor Materials

material	E_{HOMO} (eV)[a]	E_{LUMO} (eV)[a]	ΔE_{A-D} (eV)[b]	V_{OC} (V)[c]
pentacene	5.1	3.0	1.5	0.35
CuPc	5.2	3.2	1.6	0.57
NPD	5.5	1.7	1.9	0.9
C_{60}	6.2	3.6	–	–

[a] Data taken from ref 1. [b] $\Delta E_{A-D} = E^{A}_{LUMO} - E^{D}_{HOMO}$ relative to the donor C_{60} LUMO. [c] See the SI.

summarized in Table 1. As can be seen in Figure 3a, for a set of 40 nm/40 nm bilayer heterostructures on ITO, the photovoltage $\Delta\phi_{ITO/donor/C_{60}}$ (left axis) increased monotonically with the offset $\Delta E_{A-D} = E^{A}_{LUMO} - E^{D}_{HOMO}$. The absolute value of $\Delta\phi_{ITO/donor/C_{60}}$ also coincided extremely well with the measured V_{OC} values (right axis) for the respective OPV cells (see the SI). We interpret these results to mean that $\Delta\phi_{ITO/donor/C_{60}}$ reflects the difference in quasi-Fermi levels (work functions) across the heterojunctions. Previous KFM analysis of inorganic solar cells also demonstrated that KFM is sensitive to quasi-Fermi level positions.[23] Our data also support the current understanding that the D/A interface is the most prominent charge-separating interface in an OPV cell and that V_{OC} is well-correlated with the position of the HOMO level.[1]

On the basis of these results, several conclusions can be made about the Fermi level lineup across organic heterojunctions and the information provided by KFM. As shown in Figure 3b, when all of the materials in a bilayer stack are in contact, the Fermi levels align, resulting in vacuum level shifts in the dark (more on this below). *In the light*, carriers are generated when excitons split at the D/A interface, and the organic layers, which are normally insulating in the dark, become conductive. For example, illumination at ~300 mW/cm^2 results in a conductivity increase in the organic layers by roughly 7 orders of magnitude (see Figure S2d in the SI). For the ITO/NPD/C_{60} heterostructure, accumulation of electrons in the C_{60} layer raises the C_{60} quasi-Fermi level toward the LUMO band edge (shown in red in Figure 3b). The KFM probe detects the quasi-Fermi level of the illuminated C_{60} when the probe is positioned on top of the heterostructure, and of course it also detects the ITO Fermi level when it is over bare ITO (Figure 2b). Consequently, the potential difference $\Delta\phi_{ITO/donor/C_{60}}$ between the C_{60} layer and the ITO under illumination (Figure 2c) can be understood as the position of the C_{60} Fermi level relative to ITO. More explicitly, $\Delta\phi_{ITO/donor/C_{60}} = [E_{F,A}(I) - E_{F,ITO}]/e$, where I is the light intensity, $E_{F,ITO}$ is the ITO Fermi level, and $E_{F,A}(I)$ is the light-intensity-dependent quasi-Fermi level of C_{60}. It should be noted that in the ITO/donor/C_{60} structure, the quasi-Fermi level of the donor is pinned to $E_{F,ITO}$ because the donor is in direct contact with ITO.

Interpretation of the KFM data *in the dark* is a bit more subtle. As mentioned above, the organic layers are insulating in the dark. The KFM probe thus couples firmly to the conductive ITO substrate, where the Fermi level is well-defined. That is, KFM does not sense the work functions (Fermi levels) of the donor or acceptor materials in the dark but rather detects the work function of the ITO underneath the organic overlayers. Vacuum level shifts due to the organic overlayers are detected as changes in the work function of the underlying ITO. The importance of this conclusion is that it means that the light and dark curves in Figure 2b are fundamentally different. In the light, ϕ measures the Fermi level of C_{60}, but in the dark, ϕ reflects $E_{F,ITO}$. We believe

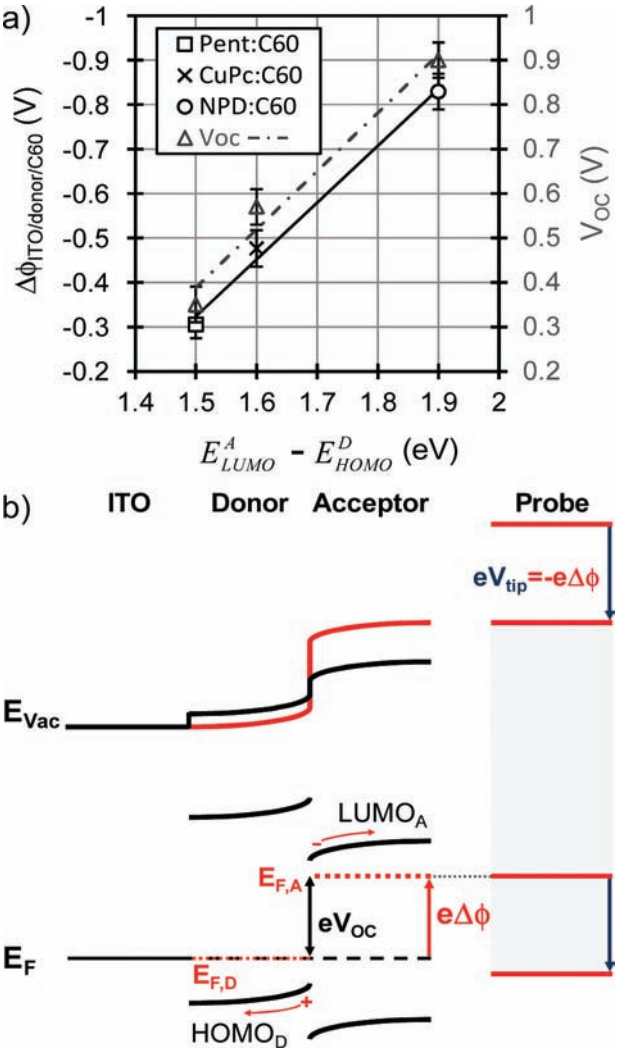

Figure 3. (a) C_{60} potentials at ~300 mW/cm^2 illumination for a series of donor (40 nm)/C_{60} (40 nm) heterostructures deposited on ITO. Plotting the C_{60} potential $\Delta\phi_{ITO/donor/C_{60}}$ (left axis) and the device V_{OC} (right axis) as functions of the HOMO/LUMO offset of the D/A material reveals a monotonic increase in the photovoltage (solid line) that is correlated with the increase in V_{OC} (dashed line). The error bars represent 95% confidence intervals [two standard deviations ($\pm 2\sigma$) from the mean]. (b) Energy level alignment diagram across an ITO/D/A stack in the dark along with the KFM probe. In the dark, the Fermi levels for all of the materials align, resulting in vacuum level shifts. Under illumination, excitons split at the D/A interface with electron buildup in C_{60}. Under intense illumination, the free charge carriers split the D/A Fermi levels into quasi-states (red dashed lines). The quasi-Fermi level ($E_{F,D}$) of the donor layer becomes pinned to the ITO Fermi level after hole extraction, and electron accumulation in the acceptor layer shifts its quasi-Fermi level ($E_{F,A}$) upward. The Kelvin probe senses this as a shift in the work function of the acceptor layer, allowing $E_{F,A}$ to be tracked under illumination.

that $\Delta\phi_{ITO/donor/C_{60}}$ as defined above reflects the photogenerated electrochemical potential, which is directly comparable to V_{OC} (i.e., we do not subtract the dark curve from the light curve). This analysis is strongly supported by the one-to-one correlation observed between $\Delta\phi_{ITO/donor/C_{60}}$ and V_{OC} in Figure 3a.

Thus, KFM measurements yield the quasi-Fermi level for the exposed C_{60} layer under illumination. This Fermi level is

measured relative to the donor quasi-Fermi level, which is pinned to the grounded ITO contact. Because KFM measures $E_{F,A} - E_{F,D}$, the splitting of the quasi-Fermi levels across the D/A interface, it provides the maximum photopotential that a given D/A pair can generate. That is, $E_{F,A} - E_{F,D}$ represents how much the D/A interface can energetically "pump" electrons (and holes) in an OPV cell.

In conclusion, we have demonstrated a direct correlation between V_{OC} values for organic heterostructures and photovoltages measured by KFM. We have found that KFM can selectively track the quasi-Fermi levels of organic layers for different heterojunctions. Overall, these results demonstrate that KFM is a useful tool for understanding photovoltaic effects in organic heterostructures and may be used in conjunction with other scanning probe microscopy techniques designed to probe OPV materials.[24−28] Future work will focus on understanding photovoltages for other D/A combinations, the influence of different contact metals, the importance of dark-state (built-in) CPDs, the effect of interfacial blocking layers, and the role of film morphology, for example.

■ ASSOCIATED CONTENT

Supporting Information. Light spectra, OPV data, KFM of ITO/pentacene/C_{60} and ITO/CuPc/C_{60} bilayers, statistical analysis of the layer potential difference, and experimental details. This material is available free of charge via the Internet at http://pubs.acs.org.

■ AUTHOR INFORMATION

Corresponding Author
frisbie@umn.edu

■ ACKNOWLEDGMENT

This work was partially supported by the MRSEC Program of the National Science Foundation under DMR-0819885 and by the NSF through DMR-0706011. We thank Prof. Russell Holmes and Prof. Paul Ruden for critical reading of the manuscript.

■ REFERENCES

(1) Rand, B. P.; Burk, D. P.; Forrest, S. R. *Phys. Rev. B* **2007**, *75*, No. 115327.
(2) Scharber, M.; Wuhlbacher, D.; Koppe, M.; Denk, P.; Waldauf, C.; Heeger, A. *Adv. Mater.* **2006**, *18*, 789.
(3) Koch, N. *ChemPhysChem* **2007**, *8*, 1438.
(4) Mihailetchi, V. D.; Blom, P. W. M.; Hummelen, J. C.; Rispens, M. T. *J. Appl. Phys.* **2003**, *94*, 6849.
(5) Lo, M. F.; Ng, T. W.; Liu, T. Z.; Roy, V. A. L.; Lai, S. L.; Fung, M. K.; Lee, C. S.; Lee, S. T. *Appl. Phys. Lett.* **2010**, *96*, No. 113303.
(6) Hwang, J.; Wan, A.; Kahn, A. *Mater. Sci. Eng., R* **2009**, *64*, 1.
(7) Zhu, X.; Kahn, A. *MRS Bull.* **2010**, *35*, 443.
(8) Gregg, B. A.; Hanna, M. C. *J. Appl. Phys.* **2003**, *93*, 3605.
(9) Wagenpfahl, A.; Rauh, D.; Binder, M.; Deibel, C.; Dyakonov, V. *Phys. Rev. B* **2010**, *82*, No. 115306.
(10) Nonnenmacher, M.; O'Boyle, M. P.; Wickramasinghe, H. K. *Appl. Phys. Lett.* **1991**, *58*, 2921.
(11) Fujihira, M. *Annu. Rev. Mater. Sci.* **1999**, *29*, 353.
(12) Jacobs, H. O.; Knapp, H. F.; Stemmer, A. *Rev. Sci. Instrum.* **1999**, *70*, 1756.
(13) Muller, E. M.; Marohn, J. A. *Adv. Mater.* **2005**, *17*, 1410.
(14) We note that this light spectrum is different from that of a solar simulator (see Figure S1 in the SI). However, we used it here as a proof-of-concept because it was readily available in our current setup.
(15) Peumans, P.; Forrest, S. R. *Appl. Phys. Lett.* **2001**, *79*, 126.
(16) Khshto, G. P.; Kim, W.; Kafafi, Z. H. *Appl. Phys. Lett.* **2005**, *86*, No. 093502.
(17) Milliron, D. J.; Hill, I. G.; Shen, C.; Kahn, A.; Schwartz, J. *J. Appl. Phys.* **2000**, *87*, 572.
(18) Vázquez, H.; Gao, W.; Flores, F.; Kahn, A. *Phys. Rev. B* **2005**, *71*, No. 041306.
(19) Wang, Z. B.; Helander, M. G.; Greiner, M. T.; Qiu, J.; Lu, Z. H. *Appl. Phys. Lett.* **2009**, *95*, No. 043302.
(20) Sze, S. M. *Physics of Semiconductor Devices*; Wiley: New York, 1981 (Schottky diodes).
(21) Koster, L. J. A.; Mihailetchi, V. D.; Ramaker, R.; Blom, P. W. M. *Appl. Phys. Lett.* **2005**, *86*, No. 123509.
(22) Chiesa, M.; Burgi, L.; Kim, J.; Shikler, R.; Friend, R. H.; Sirringhaus, H. *Nano Lett.* **2005**, *5*, 559.
(23) Jiang, C.; Moutinho, H. R.; Friedman, D. J.; Geisz, J. F.; Al-Jassim, M. M. *J. Appl. Phys.* **2003**, *93*, 10035.
(24) Coffey, D.; Ginger, D. *Nat. Mater.* **2006**, *5*, 735.
(25) Pingree, L.; Reid, O.; Ginger, D. *Nano Lett.* **2009**, *9*, 2946.
(26) Pingree, L.; Reid, O.; Ginger, D. *Adv. Mater.* **2009**, *21*, 19.
(27) Dante, M.; Peet, J.; Nguyen, T. *J. Phys. Chem. C* **2008**, *112*, 7241.
(28) Dante, M.; Garcia, A.; Nguyen, T. *J. Phys. Chem. C* **2009**, *113*, 1596.